Nanoparticle Shape Conservation in the Conversion of MnO Nanocrosses into Mn_3O_4

Irene Rusakova,[†] Teyeb Ould-Ely,[‡] Cristina Hofmann,[‡] Darío Prieto-Centurión,[‡] Carly S. Levin,[‡] Naomi J. Halas,[‡,§] Andreas Lüttge,[‡,||] and Kenton H. Whitmire*[,‡]

Texas Center for Superconductivity, University of Houston, Houston, Texas 77204-5931, Department of Chemistry and the Center for Biological and Environmental Nanotechnology, MS 60, Rice University, 6100 Main Street, Houston, Texas 77005, Department of Electrical and Computer Engineering, MS 366, Rice University, 6100 Main Street, Houston, Texas 77005, and Department of Earth Science, MS 126, Rice University, 6100 Main Street, Houston, Texas 77005

Received November 7, 2006. Revised Manuscript Received January 22, 2007

The conversion of hexagonal-, square-, and cross-shaped MnO nanoparticles into mixed MnO−Mn_3O_4 nanoparticles occurs with retention of the nanoparticle shape. Upon aging, extra diffraction spots appear in the TEM analyses of both hexagonal- and cross-shaped nanoparticles (NPs). These extra diffraction spots can be assigned to the spinel form of Mn_3O_4 (s-Mn_3O_4) and exhibit moiré interference patterns arising from the presence of two closely aligned, crystallographically similar phases. Examination of a variety of reaction conditions showed that the transformation of MnO into MnO/Mn_3O_4 occurred while the particles are suspended in hexane at ambient temperature, by refluxing in hexadecane for 36 h, by heating to 200 °C in air, and by irradiating the NPs with a Raman laser beam. The crystal phase development and shape retention can be observed by using transmission electron microscopy (TEM). Single-crystal and polycrystalline selected area electron diffraction (SAED) patterns and dark-field TEM images confirm the coexistence of both MnO and s-Mn_3O_4 phases. Evaluation of the polycrystalline SAED patterns after irradiation in the Raman spectrometer indicated the presence of rings assignable to the tetragonal phase of Mn_3O_4 (t-Mn_3O_4) as well as MnO and s-Mn_3O_4. The growth of the tetragonal phase by laser heating in the Raman experiment was confirmed by powder X-ray diffraction.

Introduction

Shape control of nanoparticles (NPs) is very desirable due to the effects that the structural anisotropy can have on various physical properties such as optical, magnetic, and electronic properties.[1−3] Because of these size- and shape-dependent properties, much effort has been employed in controlling NP morphology and assembling NPs into 2D and 3D structures.[4,5] Manganese oxides, in particular, have attracted attention because of their applications in catalysis and energy storage.[4−8]

The synthesis of MnO NPs that produces classical shapes such as nanocubes, nanospheres, or nanorods is performed by decomposition of a metal carboxylate in an organic template solution.[6−9] Unusual MnO shapes such as nanohexapods and nanocrosses have been successfully synthesized via sol−gel processes.[10,11] In contrast to the MnO growth mechanism proposed by others,[10] we have shown that the formation of MnO nanocross-shaped particles results from development of a negative energy curvature on the {110} faces, which leads to the formation of tunnels and ultimately to dendritic growth at the corners of a nanocube.[11] The shaping phenomenon takes place by an etching process and/or return to a two-dimensional growth mechanism. Several parameters such as the presence of O_2, concentration of H_2O, reaction time, reaction temperature, surfactant nature, pH, and solution viscosit, affect the etching and growth mechanisms.

In this paper we report the controlled conversion of MnO nanocrosses and nanohexagons into MnO−Mn_3O_4 while retaining NP shape. As far as we know, oxide ion intercala-

* To whom correspondence should be addressed. E-mail: whitmir@rice.edu. Tel.: 713-348-5650. Fax: 713-348-5155.
[†] University of Houston.
[‡] Department of Chemistry and the Center for Biological and Environmental Nanotechnology, Rice University.
[§] Department of Electrical and Computer Engineering, Rice University.
[||] Department of Earth Science, Rice University.

(1) Jun, Y.; Choi, J.; Cheon, J. *Angew. Chem., Int. Ed.* **2006**, *45*, 3414−3439.
(2) (a) Yin, Y.; Alivisatos, A. P. *Nature* **2005**, *437*, 664−670. (b) Buhro, W. E.; Colvin, V. L. *Nature Mater.* **2003**, *2*, 138−139. (c) Sun, Y.; Xia, Y. *Science* **2002**, *298*, 2176−2179.
(3) (a) Narayanan, R.; El-Sayed, M. A. *Nano Lett.* **2004**, *4*, 1343−1348. (b) Zhong, X.; Feng, Y.; Lieberwirth, I.; Knoll, I. *Chem. Mater.* **2006**, *18*, 2468−2471. (c) Zhou, S.; McIlwrath, K.; Jackson, G.; Eichhorn, B. *J. Am. Chem. Soc.* **2006**, *128*, 1780−1781.
(4) Yuan, J.; Li, W.-N.; Gomez, S.; Suib, S. L. *J. Am. Chem. Soc.* **2005**, *127*, 14184−14185.
(5) Cheon, J.; Kang, N.-J.; Lee, S.-M.; Lee, J.-H.; Yoon, J.-H.; Oh, S. J. *J. Am. Chem. Soc.* **2004**, *126*, 1950−1951.
(6) Brock, S. L.; Duan, N.; Tian, Z. R.; Giraldo, O.; Zhou, H.; Suib, S. L. *Chem. Mater.* **1998**, *10*, 2619−2628.
(7) Seo, W. S.; Jo, H. H.; Lee, K.; Kim, B.; Oh, S. J.; Park, J. T. *Angew. Chem., Int. Ed.* **2004**, *43*, 1115−1117.
(8) Yin, M.; O'Brien, S. *J. Am. Chem. Soc.* **2003**, *125*, 10180−10181.
(9) Park, J.; Kang, E.; Bae, C. J.; Park, J.-G.; Noh, H.-J.; Kim, J.-Y.; Park, J.-H.; Park, H. M.; Hyeon, T. *J. Phys. Chem. B* **2004**, *108*, 13594−13598.
(10) (a) Zitoun, D.; Pinna, N.; Frolet, N.; Belin, C. *J. Am. Chem. Soc.* **2005**, *127*, 15034−15035. (b) Zhong, X.; Xie, R.; Sun, L.; Lieberwirth, I.; Knoll, W. *J. Phys. Chem. B* **2006**, *110*, 2−4.
(11) Ould-Ely, T.; Prieto-Centurion, D.; Kumar, A.; Guo, W.; Knowles, W. V.; Asokan, S.; Wong, M. S.; Rusakova, I.; Lüttge, A.; Whitmire, K. H. *Chem. Mater.* **2005**, *18*, 1821−1829.

10.1021/cm062649u CCC: $37.00
Published on Web 02/27/2007

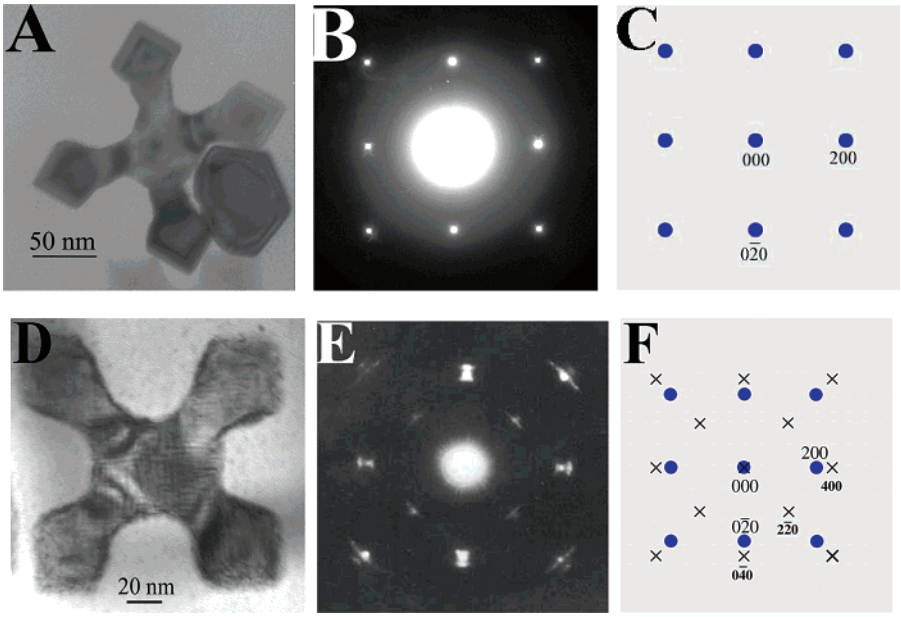

Figure 1. TEM images were taken at [001] zone axes: (A) BF TEM image of a fresh nanocross. (B−C) Experimental and simulated SAED patterns confirming the fcc-MnO lattice. (D) BF TEM image of an aged nanocross. (E−F) Experimental and simulated (at [001] zone axis orientation) SAED patterns showing two sets of distinct diffraction spots attributed to MnO and s-Mn_3O_4. Larger font indices in (F) indicate MnO (●) and the smaller font indices indicate s-Mn_3O_4 (×).

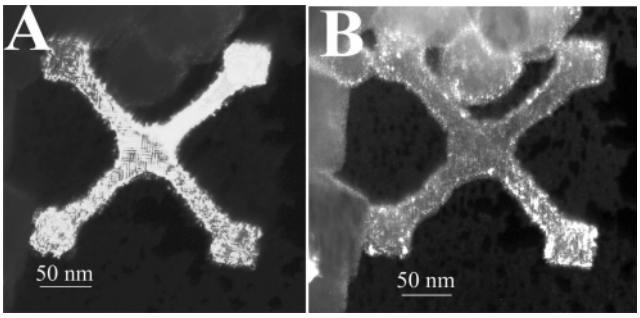

Figure 2. DF TEM images of a single nanocross using either (A) $\mathbf{g}_{MnO}$ = 2$\bar{2}$0 or (B) $\mathbf{g}_{s-Mn_3O_4}$= 220. The bright areas in (A) are MnO, while those in (B) are s-Mn_3O_4.

tion of this type has not been previously reported. This can be compared to the finding of Kido et al. who reported the topotactic growth of a Cr_2O_3 layer on the surface of α-Cr nanoparticles.[12] Cadmium selenide nanocrystals were found to undergo reversible cation exchange upon treatment with silver nitrate solutions.[13] The spherical shape of these nanoparticles was retained throughout that process. Others observed that substitution of cadmium in CdSe by Cu^{2+}, In^{3+}, Ni^{2+}, and Co^{2+} in addition to Ag^{+} led to changes in catalytic activity of the particles; however, the morphology of the nanoparticles after substitution was not reported.[14] In contrast to the finding presented here for MnO, oxidation of spherical Fe_3O_4 nanoparticles resulted in formation of rod-shaped γ-Fe_2O_3.[15]

(12) Kido, O.; Kamitsuji, K.; Kurumada, M.; Sato, T.; Kimura, Y.; Suzuki, H.; Sait, Y.; Kaito, C. *J. Cryst. Growth* **2005**, *275*, e1745−e1750.
(13) Son, D. H.; Hughes, S. M.; Yin, Y.; Alivisatos, A. P. *Science* **2004**, *2004*, 1009−1012.
(14) Kapinus, I. E.; Viktorova, T. I.; Khalyavka, T. A. *Theor. Exp. Chem.* **2006**, *42*, 282−286.
(15) Kang, Y. S.; Risbud, S.; Rabolt, J. F.; Stroeve, P. *Chem. Mater.* **1996**, *8*, 2209−2211.

Experimental Section

The synthesis of MnO ($Fm\bar{3}m$ structure, a = 0.445 nm) nanocrystals was done following the same process described in the literature.[11] In this methodology, managese(II) formate is decomposed at 340 °C in a mixture of tri-*N*-octylamine (TOA) and oleic acid (OA) with small amounts of added water. The relative amounts of TOA/OA/H_2O determine the morphology of the resultant nanoparticles.

Transformation in Hexane. After NP synthesis, the NP-surfactant slurry was suspended in hexane and left standing in contact with air at ambient temperature. Hexagonal-, square-, or cross-shaped particles were treated the same. The NP suspensions turned from green to brown in less than 1 h. After 48 h an aliquot was diluted to give an almost colorless suspension which was used to prepare the TEM samples. To obtain a dry powder for XRD measurements, a suspension of NPs in hexane was sonicated, centrifuged, decanted, and dried under vacuum. This process was repeated until a loose dry powder was obtained.

Transformation in Refluxing Hexadecane. Fresh NPs were dried (vide supra), suspended in hexadecane, and refluxed (b.p. 287 °C) with vigorous stirring for 36 h in air. Then they were washed with hexane and dried following the process mentioned above.

Transformation upon Heating in Air. About 0.25 g of a newly dried NP powder was placed in an open ceramic boat. The boat was placed inside a tube furnace open to air and the sample was heated to the desired temperature for several hours (4−6 h). The sample was cooled to room temperature and ground for powder XRD analysis. The process was repeated to obtain data for different annealing temperatures.

Transformation in the Raman Laser Beam. Nearly 20 mg of a newly dried sample of the NPs was prepared and analyzed on a *Renishaw inVia* micro-Raman spectrometer using a 785 nm source with a 30 × 30 μm^2 spot size. The spectra were recorded as a function of time, with each spectrum being the average of three scans. To collect enough material for XRD from the Raman irradiation process, multiple irradiations were applied in various spots, while monitoring the conversion in the Raman spectrum in air.

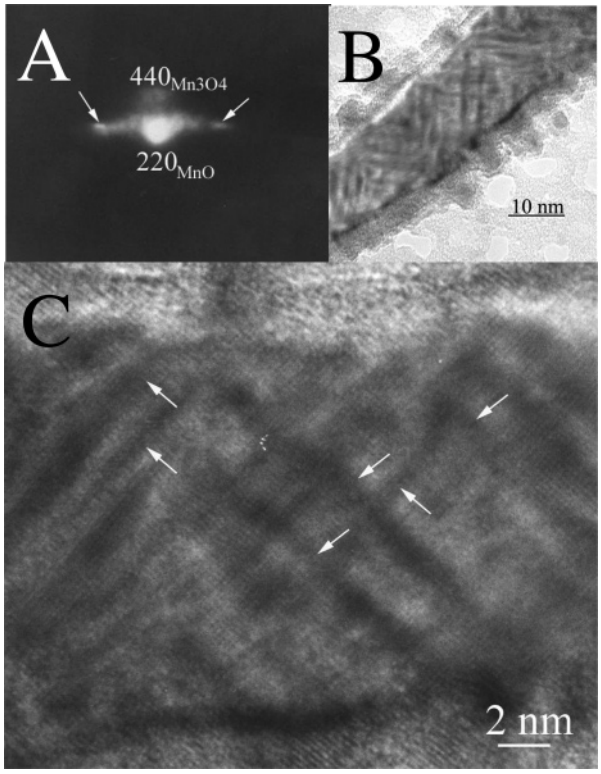

Figure 3. TEM images showing the overall moiré interference pattern: (A) An enlarged section of Figure 1E showing the simultaneous occurrence of the 440 reflection of s-Mn_3O_4 near the 220 reflection of MnO. Streaking caused by double diffraction is indicated by the arrows. The slight curvature of the streak is caused by deviation of atomic planes from their ideal alignment. (B) A TEM image of a section of a nanocross arm. (C) An HR TEM of the nanocrystal section shown in (B) indicating atomic planes and both rotational and translational moiré. (Some of the moiré fringes are indicated by arrows.)

TEM Studies. The TEM studies were carried out using JEOL 2000FX and JEOL 2010 microscopes equipped with energy-dispersive spectrometers and operated at 200 kV. Conventional and high-resolution (HR) TEM imaging, selected area electron diffraction (SAED), and energy-dispersive spectroscopy (EDS) methods were used. Precautions have been taken to minimize structural changes in the studied material caused by electron beam heating effects. This included lower intensity of the electron beam and minimizing the time that a given area was observed. All TEM samples were prepared from diluted suspensions in hexane.

X-ray Powder Diffraction Studies. X-ray powder diffraction (XRD) was performed on the NPs for lattice parameter and phase determination using a Rigaku D/Max Ultima II Powder Diffractometer operated at 40 kV and 40 mA with unfiltered Cu Kα radiation ($\lambda = 1.5406$ Å). All data were obtained at room temperature. Prior to the X-ray analyses, the samples were washed a minimum of three times with hexane, dried under reduced pressure, and ground to give dark powders. To follow the conversion of the MnO to Mn_3O_4 and then to Mn_2O_3 with heating, the following procedure was followed. The sample was ground and then heated to the desired temperature for 4 h, after which it was ground further and the XRD spectrum taken. After grinding again, the sample was heated to the next higher temperature. The data were collected in increments of 100 °C. The XRD pattern of the MnO nanocrosses corresponded to face-centered cubic (fcc) MnO ($Fm\bar{3}m$ (No. 225); $a = 0.445$ Å) and those of Mn_3O_4 correspond to either spinel Mn_3O_4 (s-Mn_3O_4, $Fd\bar{3}m$ (No. 227), $a = 0.842$ nm) or face-centered tetragonal Mn_3O_4 (t-Mn_3O_4, $I4_1/amd$ (No. 141), $a = 0.577$ nm, $c = 0.944$ nm).

Results and Discussion

Partial crystal phase transformation of MnO NPs occurs upon mild oxidation while the particles are suspended in hexane in air for 1 or more days. This spontaneous oxidation occurs slowly and in its early stages can be confirmed only by using TEM. Bright-field (BF) TEM images of freshly prepared nanocrosses reveal only thickness extinction fringes. No defects or other phases are detected in these samples (Figure 1A). The SAED pattern obtained from a freshly prepared single cross-shaped particle (Figures 1B and 1C) confirmed this observation. Only diffraction spots due to MnO were observed in this pattern; however, upon exposure to air (1−10 days) while suspended in hexane, the particles developed a stripe contrast (Figure 1D), which can be attributed to moiré fringes, and extra reflections in the SAED patterns (Figures 1E and 1F) were observed. Analysis of the SAED pattern shows that the extra reflections are due to formation of a second phase identified as the spinel form s-Mn_3O_4. In the fcc-MnO crystal lattice, which adopts the rock salt structure, the manganese ions are located in all of the octahedral sites, whereas in the s-Mn_3O_4 crystal lattice a fraction of both the octahedral and the tetrahedral sites is occupied. Because of the lower symmetry created by the new locations of the metal ions, the unit cell edge length *a* of the Mn_3O_4 unit cell is approximately double that of MnO (vide infra). This near doubling of the lattice parameter causes the diffraction patterns arising from both compounds to exhibit moiré fringes as described below.

Because s-Mn_3O_4 has a lattice parameter that is almost double that of MnO (0.842 vs 0.445 nm), a previous report attributed these additional diffraction spots to ⟨110⟩ reflections from the MnO lattice.[10] However, these ⟨110⟩ reflections should be systematically absent in the face-centered cubic symmetry. It is important to note that s-Mn_3O_4 forms under mild reaction conditions, which is interesting because the more stable crystal form of Mn_3O_4 is the tetragonal setting. Presumably, the choice of the cubic over the tetragonal form of Mn_3O_4 occurs because of the existing cubic close-packed oxygen lattice of the starting rock salt MnO crystal structure. As will be discussed later, heating of the NPs in a high boiling point solvent or in air forms the tetragonal phase.

Crystal DF (dark field) TEM images were recorded using $\mathbf{g}_{MnO} = 2\bar{2}0$ (Figure 2A) and $\mathbf{g}_{s-Mn_3O_4} = 220$ (Figure 2B) to view the distribution of MnO and s-Mn_3O_4 phases within a single nanocross. As may be expected, the concentration of s-Mn_3O_4 is higher near the surface and on the edges of the NPs, where oxidation occurs first. The s-Mn_3O_4 phase grows as thin plates within the MnO matrix. The plate shape of the intercalating Mn_3O_4 phase is one of the origins for streaks in the SAED patterns (Figures 1E and 3A). Another origin for streaks is the presence of planar defects (stacking faults) in the internal structure of such a complex intergrowth of two phases. The stripe contrast that has been observed on the aged nanocrosses (Figures 1D, 3B, and 3C) has a much larger periodicity than the individual or combined lattice periodicities of the MnO and s-Mn_3O_4 phases and is therefore ascribed to moiré interference patterns. In the mixed MnO/s-Mn_3O_4 nanocrosses the above-mentioned observations are

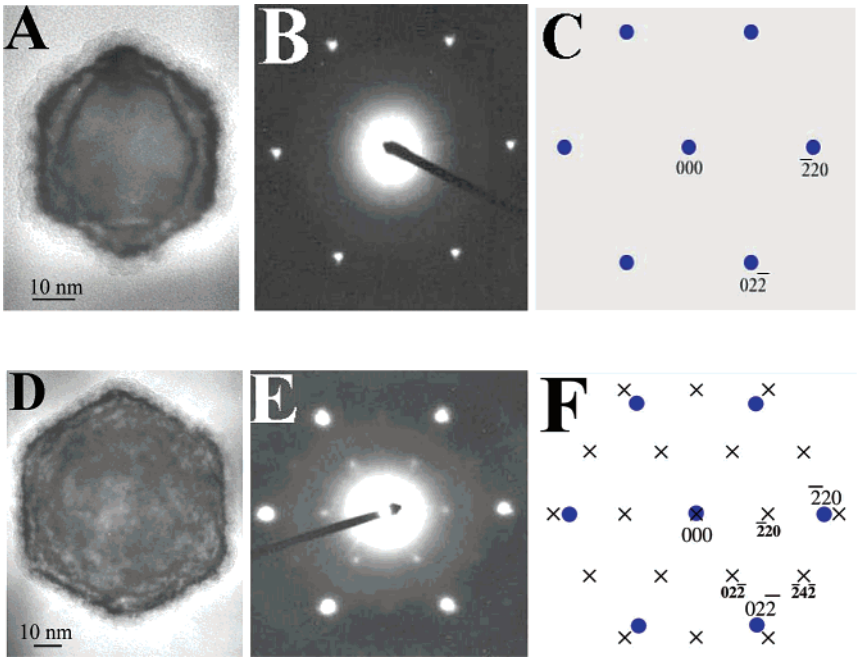

Figure 4. BF TEM images (taken at [111] zone axes) of fresh (A) and aged (D) hexagonal nanoparticles. Experimental (B) and simulated (C) SAED patterns for fresh NPs in which only the fcc-MnO phase is present. Experimental (E) and simulated (F) SAED patterns of aged NPs where fcc-MnO and s-Mn_3O_4 phases are observed. Larger font indices in (F) indicate fcc-MnO (●), while smaller font indices indicate s-Mn_3O_4 (×).

a consequence of a layered growth mechanism. Moiré patterns are observed in TEM images when overlap occurs between two crystals with almost exactly equal lattice parameters (or integral multiples thereof). In this case, both MnO and s-Mn_3O_4 have cubic close-packed lattices of oxygen atoms with Mn^{n+} ($n = 2$ or 3) ions in the interstices and, as mentioned previously, the unit cell length a for s-Mn_3O_4 is almost double that of MnO. When a material is composed of well-aligned crystals of different compounds with similar lattice parameters, moiré patterns form if a beam diffracted by both crystals is allowed to recombine with the transmitted beam to form the final image (double diffraction). There are two different types of moiré interference: translational and rotational. Both are observed in the aged NPs containing both MnO and s-Mn_3O_4. The translational moiré arises when two crystals have parallel reflecting planes and a small difference in lattice parameters. In our aged nanocrosses, such small differences occur between the second-order reflecting planes in MnO ({200} and {220}) and the fourth order reflecting planes in s-Mn_3O_4 ({400} and {440}); see Figures 1D−1F. Double diffraction in this structure is also confirmed by the presence of extra spots in the SAED patterns near the basic reflections (Figure 3A). The rotational moiré occurs when both crystals have identical spacing but a slight angular rotation, which takes place in our aged nanocrosses as well. Such angular rotation causes azimuthal deviations of streaks in the SAED patterns (Figure 3A). Other workers have observed Mn_3O_4 forming from MnO under mild conditions, for example, traces of Mn_3O_4 have been formed on the surface of rod-shaped MnO NPs,[9] but intercalated growth as found here has not been reported for shaped particles to our knowledge.

Similar conversion of MnO to Mn_3O_4 is observed in the hexagonal or square NPs whose syntheses we reported previously.[11] The corresponding images are shown in Figures 4 and 5. The images were recorded on fresh and aged nanocrystals with a ⟨111⟩ zone axis orientation for the hexagonal nanoparticles and a ⟨001⟩ zone axis for the square nanoparticles. Owing to the similarity to the hexagonal- and cross-shaped particle results, the diffraction patterns on the square nanoparticles was not investigated extensively. The additional reflections in the SAED pattern from the aged hexagonal particles are again consistent with the presence of s-Mn_3O_4.

Fresh, cross-shaped NPs were dispersed in refluxing hexadecane (287 °C) for ca. 36 h to oxidize MnO into MnO/s-Mn_3O_4 (Figure 5). The XRD spectrum confirmed the presence of MnO and, in this case, the t-Mn_3O_4 phase. This is to be expected since the thermodynamically stable form of Mn_3O_4 is the tetragonal phase, which would be expected to form upon thermal treatment of MnO.

The XRD patterns on heated powder samples of the NPs (Figure 6) confirm the partial conversion of MnO to t-Mn_3O_4 above 200 °C. Above 400 °C the oxidation process leads to Mn_2O_3 which has not yet been observed for the mild oxidation of the hexagonal- and cross-shaped NPs. From 200−400 °C the XRD peaks are broad, indicating poor crystallinity or the existence of very small crystal domains in the Mn_3O_4 phase. This is consistent with the TEM data where in situ heating to >400 °C of both the hexagonal- and cross-shaped nanoparticles led to loss of the moiré interference patterns and other changes in the SAED patterns that indicated a further transformation to an amorphous material. When they were heated to above 500 °C, the XRD pattern showed highly crystalline single-phase Mn_2O_3.

Raman spectroscopy was initially intended to identify and differentiate between the MnO and the Mn_3O_4 phases. It was noticed though when irradiating a fresh sample of the MnO nanocrosses with moderate laser beam intensity (0.07 mW) that further conversion of MnO to Mn_3O_4 occurred

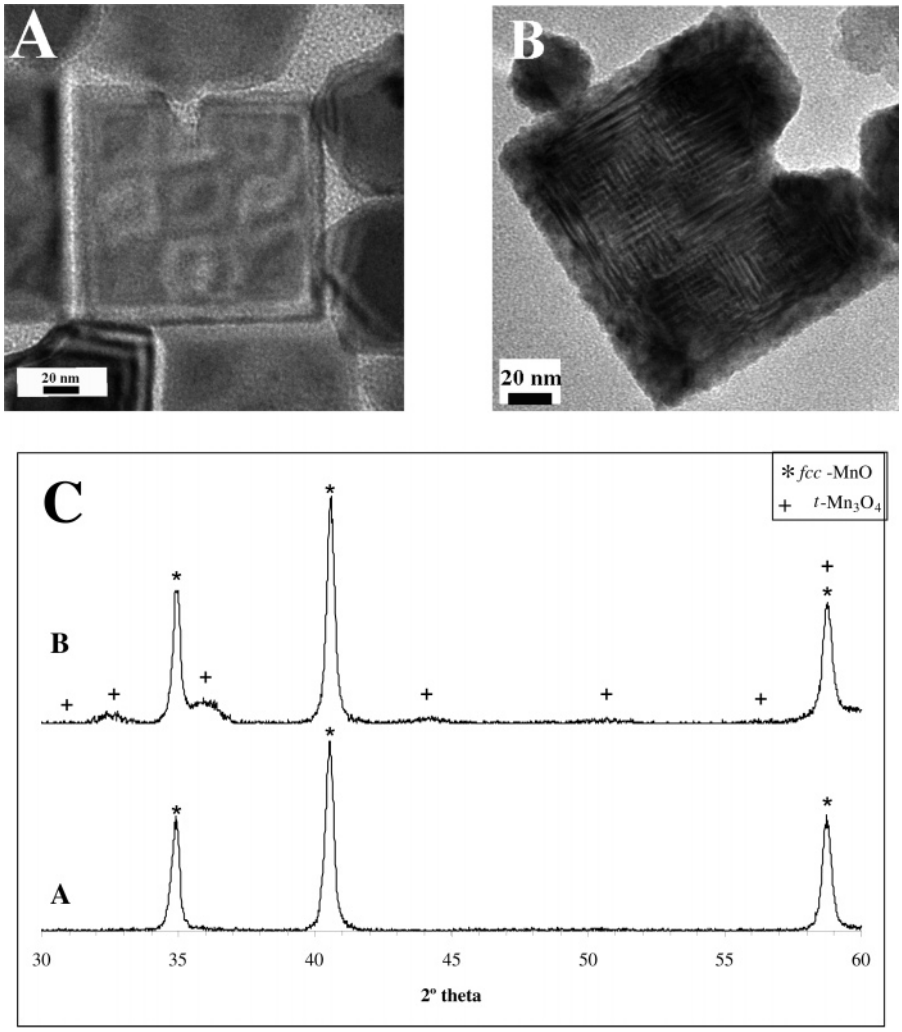

Figure 5. TEM images of (A) freshly prepared MnO NPs and (B) an MnO NP after refluxing in hexadecane for 36 h in air. (C) The XRD patterns corresponding to the nanoparticles prepared in (A) and (B). The XRD trace A shows pure fcc-MnO while B shows a mixture of fcc-MnO and t-Mn_3O_4.

(Figure 7). The phase of Mn_3O_4 formed under these circumstances has been investigated and those findings will be reported separately below. The vibrational bands observed are consistent with those previously reported.[16] In this case the conversion is a function of irradiation with the laser beam, which we attribute to a local heating effect (see Experimental Section), although we cannot completely rule out photochemically induced transformations.[17−19] Both oxides, MnO and Mn_3O_4, can be observed at a beam intensity of 0.53 mW. Almost complete conversion to Mn_3O_4 is achieved by increasing the beam intensity to 1.1 mW and irradiating for a period of about 12 h. Complete conversion of the bulk sample cannot be obtained efficiently since the beam cross section covers a two-dimensional area of only $30 \times 30\ \mu m^2$ and penetration does not exceed a couple of micrometers. The irradiation process, which is comparable to heating the NPs in air, leads to a faster conversion to Mn_3O_4 than that occurring by mild oxidation in solution. Since the Raman experiments can only convert a small cross section of the sample at a time, multiple cross sections were irradiated to obtain enough material to determine the phase identity of the Mn_3O_4 obtained via laser heating.

To address the issue of the sample's bulk-phase composition, TEM polycrystalline diffraction patterns were taken before and after irradiation with the Raman laser beam (Figure 8). These SAED patterns were recorded from a large number of randomly oriented NPs. Depending on the structure factor, a number of {*hkl*} planes will reflect, and a series of concentric rings will be observed in the diffraction pattern, each corresponding to a particular set of {*hkl*} reflections. Some *d*-spacings in fcc-MnO, s-Mn_3O_4, and t-Mn_3O_4 have very similar values and cannot be distinguished using TEM ring diffraction patterns. Such rings can correspond to two (or even all three) phases being present in a given sample, so only those rings unambiguously arising from a single phase were used to confirm the presence of that phase in a given sample, and only diffraction rings at the smaller angles were indexed as they give the most accurate *d*-spacings. There is significant difference between the diffraction patterns observed in Figures 8A and 8B. Clearly, Figure 8B exhibits a much larger number of diffraction rings, consistent with the presence of t-Mn_3O_4,

(16) Julien, C. M.; Massot, M.; Poinsignon, C. *Spectrochim. Acta* **2004**, *60A*, 689−700.
(17) Shim, S.-H.; Duffy, T.S.; Jeanloz, R.; Yoo, C.-S.; Iota, V. *Phys. Rev. B* **2004**, *69*, 144107(1)−144107(12).
(18) Kramberger, C.; Waske, A.; Biedermann, K.; Pichler, T.; Gemming, T.; Buechner, B.; Kataura, H. *Chem. Phys. Lett.* **2005**, *407*, 254−259.
(19) Barshilia, H. C.; Rajam, K. S. *J. Mater. Res.* **2004**, *19*, 3196−3205.

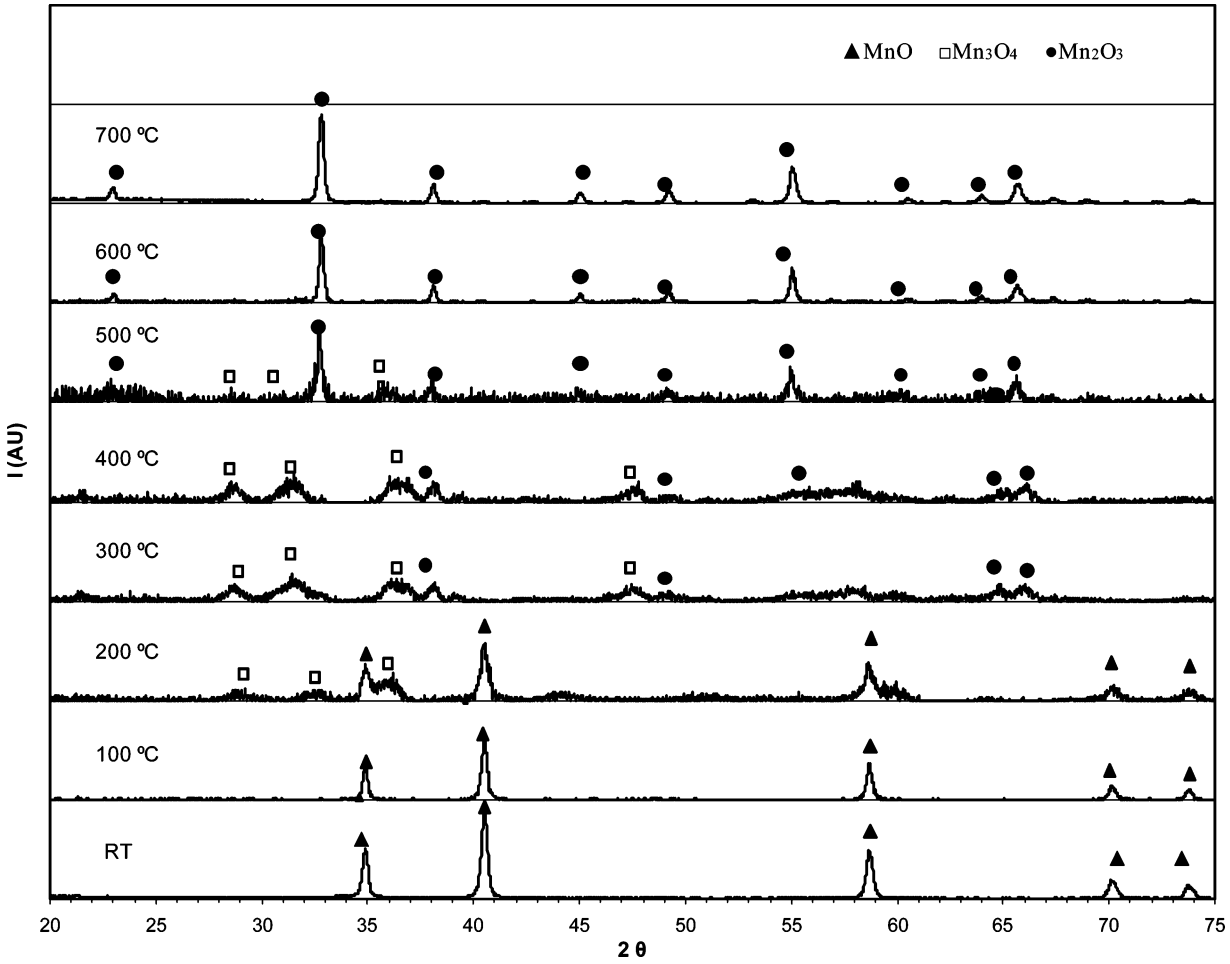

Figure 6. Change in the XRD pattern of a dry sample of the cross-shaped NPs as a function of heating temperature. The initially present fcc-MnO begins to convert to t-Mn_3O_4 above 200 °C, and Mn_2O_3 begins to appear above 300 °C.

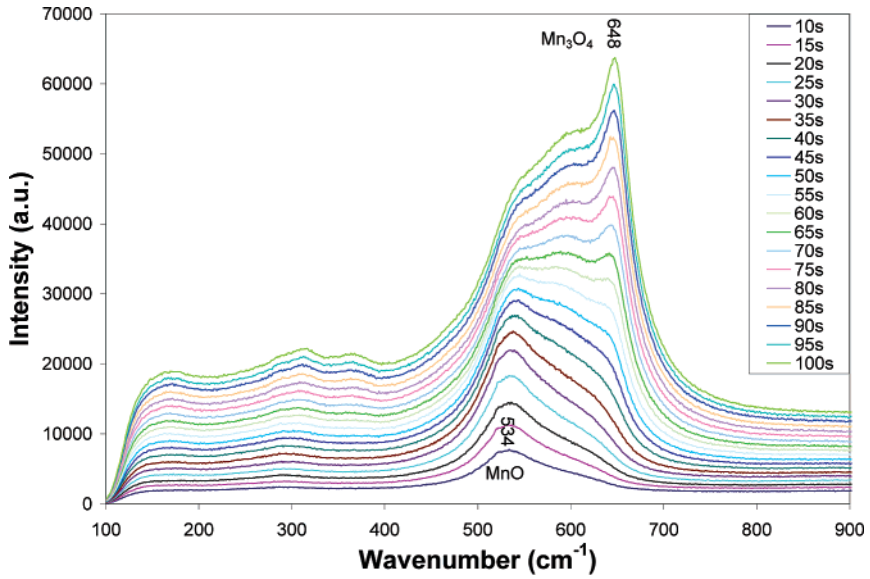

Figure 7. In situ Raman spectra reveal the evolution from pure MnO to mixed MnO/Mn_3O_4. Irradiation was ended when no further changes in the spectrum were observed.

which has a greater number of accessible *d*-spacings than MnO and s-Mn_3O_4 owing to its lower symmetry. In Figure 8A we have labeled one low-intensity ring that corresponds to s-Mn_3O_4 only, two rings from MnO only, and one from a combination of MnO and s-Mn_3O_4. Importantly, there are no rings that can be attributed to t-Mn_3O_4 in the SAED pattern. After Raman spectroscopy we observed four additional rings (Figure 8B) that can be indexed as t-Mn_3O_4. One ring was indexed as both t-Mn_3O_4 and s-Mn_3O_4, and one as a combination of MnO and s-Mn_3O_4. These results confirm our previous observations that the phase formed upon initial mild oxidation of MnO is s-Mn_3O_4, and that laser irradiation during the Raman experiment causes additional formation of Mn_3O_4 but in the tetragonal phase.

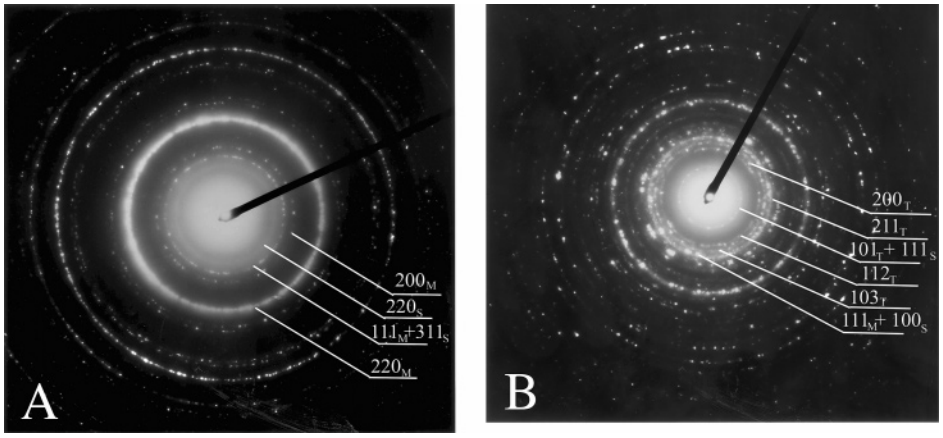

Figure 8. TEM ring diffraction patterns before (A) and after (B) irradiation with the Raman spectrometer laser beam: (A) One low-intensity ring that corresponds to s-Mn_3O_4 only (220_S), two from fcc-MnO (220_M and 200_M), one from a combination of fcc-MnO and s-Mn_3O_4 ($111_M + 311_S$). (B) Four rings correspond to t-Mn_3O_4 (200_T, 211_T, 112_T, and 103_T), one ring from both t-Mn_3O_4 and s-Mn_3O_4 ($101_T + 111_S$), and one as a combination of fcc-MnO and s-Mn_3O_4 ($111_M + 100_S$).

Note that a small amount of s-Mn_3O_4 persists in the sample. The XRD pattern of the NPs after extensive Raman laser irradiation confirmed the presence of MnO and a small amount of t-Mn_3O_4.

Conclusions

In summary, we have investigated the phase transformation of MnO nanocrosses to the mixed MnO/s-Mn_3O_4 phase and confirmed that the nanocrosses retain their shape during the initial, mild conversion. The presence of the s-Mn_3O_4 phase explains the development of additional diffraction spots in the TEM diffraction images of the cross-shaped nanoparticles, contrary to a previous report.[10a] The transformation occurs slowly in solution at room temperature when the particles are exposed to air; however, diffraction spots indexing to s-Mn_3O_4 are completely absent only in samples that are prepared immediately prior to TEM analysis. The conversion to Mn_3O_4 is also initiated on fresh samples by heating these in a high boiling point solvent, by heating the dry sample in a furnace to ca. 200 °C, or by irradiating the NPs with a Raman laser beam, but in these cases the phase formed is tetragonal Mn_3O_4. The conversion of cubic MnO to s-Mn_3O_4 was only achieved upon oxidation in air while suspended in hexane at ambient temperature. The presence of s-Mn_3O_4 as the initial product of mild oxidation of MnO and t-Mn_3O_4 as the product of Raman-irradiated samples was established by TEM SAED patterns. The oxidation sensitivity of the nanoparticles is attributed to the layered structure observed. Similar results were observed for hexagonal- and square-shaped nanoparticles as well. The ability to oxidize these shaped nanoparticles, while retaining shape, through a variety of methods is significant for their incorporation in advanced materials.

Acknowledgment. The authors would like to thank the Robert A. Welch Foundation (C-0976) and the National Science Foundation through the Center for Biological and Environmental Nanotechnology (CBEN, EEC-0647452) as well as the Texas Center for Superconductivity at the University of Houston (T_CSUH) for their financial support. We also appreciate our productive discussions with Drs. M. Pankova from TsNIIChM (Moscow) and M. Iliev and J. Meen from T_CSUH. C.S. Levin was supported by a training fellowship from the Keck Center Nanobiology Training Program of the Gulf Coast Consortia, NIH Grant No. 1 T90 DK070121-01.

Supporting Information Available: Diagrams of the MnO and s-Mn_3O_4 lattices. This information is available free of charge via the Internet at http://pubs.acs.org.

CM062649U